Extraction of humic acid from peat and lignite and the thermal behavior of their mixtures with ammonium nitrate

Dominik Nieweś[1] · Marcin Biegun[1] · Marta Huculak-Mączka[1] · Kinga Marecka[1] · Maciej Kaniewski[1] ·
Jakub Zieliński[1] · Józef Hoffmann[1]

Abstract

Due to the positive effect on soil structure and the influence on improving the efficiency of plant roots nutrient uptake, humic acids (HA) are widely considered for fertilizer production. Especially, it seems to be particularly promising to use them as additives in technologies of mineral fertilizer production. One of the common mineral fertilizer components, due to its good water solubility and the presence of nitrogen in two forms, is ammonium nitrate (AN). The aim of this study was to determine the influence of the humic acids extracted from peat and lignite on the thermal decomposition of HA and the thermal decomposition of ammonium nitrate and humic acids mixtures. For the quality assessment of HA, spectroscopic methods (FTIR/ATR and CP/MAS ^{13}C NMR) and analysis of elemental composition were used. The analysis of the spectra showed differences in the degree of humification of humic acids extracted from various raw materials. HA isolated from peat were distinguished by the presence of peptides, polysaccharides, and lignin residues. Elemental analysis showed the higher carbon and sulfur content in the extracted HA compared to the reference samples. The results of the TG-DTA-MS analysis confirmed the influence of differences in the molecular structure of humic acids, especially in the aliphatic and aromatic carbon content, on the thermal decomposition process. Total content of carboxylic and/or hydroxylic functional groups had a significant impact on the start of the decomposition temperature. Their increase visibly influenced the acceleration of the exothermic decomposition of AN.

Keywords Humic acids · Ammonium nitrate · Organic raw materials · Thermal analysis · Decomposition

Introduction

The dynamic growth of the population forces undertaking measures to increase the scale of food production. A major challenge associated with intensification of agricultural production is to successively increase crop yields and the associated provision of adequate fertilization. However, due to the negative impact of excessive fertilization on the environment, it seems necessary to ensure high fertilizer use efficiency (FUE), especially nitrogen fertilizers [1]. One of the important factors, that allows to achieve a high potential of an applied fertilizer, is appropriate conditions of soil. The soil structure affects the adsorption mechanism

of ammonium nitrogen (NH_4^+). Furthermore, the leaching of nitrates (NO_3^-), resulting from ammonium nitrification and water infiltration, also depends on the soil texture [2, 3]. In addition to providing adequate fertilization and irrigation level, soil organic matter (SOM) is important in maintaining a proper soil structure while protecting it from a degradation caused by an extensive cultivation process [4].

The SOM supplementation is an important aspect of sustainable agriculture. It can be achieved by incorporating humic acids (HA) into the soil structure, which are one of the main components of SOM. Additionally, the use of humic acids prevents the negative impact of excessive salinity in the soil, which can be caused by the use of mineral fertilizers [5]. The positive effect of HA fertilization on the yields of different types of plants has been widely discussed in the literature [6–9]. Possible use of humic acids extracted from various carbon raw materials in commercial fertilizer production technologies has been demonstrated, however, in this aspect, some difficulties have also been pointed out,

✉ Marcin Biegun
  marcin.biegun@pwr.edu.pl

1 Department of Engineering and Technology of Chemical Processes, Wrocław University of Science and Technology, Smoluchowskiego 25, 50-372 Wroclaw, Poland

especially in the context of granular fertilizer technology [10, 11].

One of the chemical compounds that is widely used in the production of nitrogen fertilizers, is ammonium nitrate (AN). Its popularity in this aspect is due to the presence of nitrogen in two forms: ammonium and nitrate [12]. Among the most frequently discussed problems with its use in the literature is the risk of the explosive decomposition of systems containing ammonium nitrate [13–16]. In recent years, many studies have been carried out to determine the thermal stability of ammonium nitrate and the influence of various additives on its explosive decomposition process. Some of these studies included analyses of ammonium nitrate mixtures with additives with fertilization potential (e.g. sulfates, potassium salts and micronutrients) [17–20]. In the industrial production of solid nitrogen fertilizers based on ammonium nitrate, carbonates are commonly used as an inhibitor of their decomposition [21, 22]. However, producing mixtures of ammonium nitrate with humic acids limits the potential for carbonates addition, especially calcium and magnesium compounds, because they significantly reduce the ion-exchange activity of humic acids. Presence of calcium or magnesium cations in the systems causes them to combine with functional groups (e.g. carboxyl, phenolic, etc.) in the humic structure and produce forms that are insoluble in the soil solution [23].

The thermal stability of humic substances extracted from various raw materials has been widely reported in recent years. In general, the carbon structure of these macromolecular organic substances is quite stable at temperature values characteristic of the technological processes of the production of granular fertilizers.

A broad decomposition of HA has been typically observed between 110 and 600 °C. It results in the formation of carbon dioxide, carbon oxide and methane which are the decomposition products of carboxyl, carboxylate, aromatic structures and the break of aliphatic chains [10, 24–26]. Signals above 600 °C, which are characteristic of mineral contamination decomposition (e.g. carbonates), can also be observed [27]. Usually, a slight loss of mass below 100 °C that is noticed is attributed to the water desorption from the HA structure. According to Kolokassidou et al., dehydration of humic acids that takes place above 70 °C may be irreversible and lead to condensation of the polyaromatic structures of humic acids [28].

The addition of organic compounds to ammonium nitrate usually results in a significant reduction of the temperature of the decomposition beginning, but in the case of the addition of humic acids, the process may also depend on their chemical structure and the type of raw material from which they were extracted [29]. This article presents and discusses the results of qualitative analyses of humic acids extracted from peat and lignite, which were compared with reference samples. Particular emphasis was placed on the thermal decomposition of extracted humic acids and their mixtures with ammonium nitrate in different mass ratios. The aim of these studies was to evaluate the relationship between the origin and molecular composition of HA and the thermal stability of ammonium nitrate. The combination of classical spectroscopic methods for the analysis of the structure of humic acids with thermal analysis of the decomposition of systems of humic acids with ammonium nitrate made it possible to determine the influence of the content of carbon atoms in forms in the structure of HA on the course of the thermal decomposition of ammonium nitrate with the addition of these substances. The safety of using HA as additives in fertilizers containing ammonium nitrate was also evaluated.

Experimental

Materials

In the presented work, humic acids that were extracted from peat (HA-P) and lignite (HA-L) were examined. Raw materials that were used for the extraction of humic acids, were derived from Polish deposits: the peatland in Żuławy district and the Bełchatów lignite mine, respectively. HA was isolated according to the IHSS method described by Trubetskaya et al., [30] with some modifications. Our procedure, with details, was described in the Methods section (humic acids extraction procedure). Solutions that were necessary for the HA isolation process were prepared with the use of NaOH and HCl purchased from POCH (Avantor Performance Materials). The results of qualitative analysis of the obtained HA were compared with the results received for reference samples that were humic acids (HA-SA-A) and their sodium salts (HA-SA-S) purchased from Sigma-Aldrich. Samples for thermal analysis were prepared with the use of ammonium nitrate purchased from EUROCHEM (purity ≥ 99.0 mass%).

Methods

Humic acids extraction procedure

According to the IHSS method, the peat and lignite samples were ground into 2 mm grains. Next, the raw material samples were decalcified. In that step, 40 g of peat or lignite were placed in a 1 L polypropylene bottle and mixed with approximately 30 mL of 1 M HCl, for acidification to pH 2. Then, 0.1 M HCl was added to the final ratio of the solution to the mass of the raw material equal to 10:1. Decalcification was carried out by shaking the suspension for 1 h and the

supernatant was separated from the solid phase by centrifugation (15 min at 1500 rpm). Subsequently, the raw material residue was neutralized to pH 7 with the use of 1 M NaOH. The alkaline extraction step included the use of 0.1 M NaOH and the mass ratio of extractant to raw material was equal to 10:1. Then, the suspension was shaken for 4 h and the phases were separated by centrifugation (15 min at 1500 rpm). The extractant was acidified with 6 M HCl to pH 1 and left for about 16 h for the precipitation of humic acids. The phases were then separated by filtration and the humic acids gel was dried at 62 °C to achieve a constant sample mass.

FTIR spectroscopy

Functional groups that were characteristic for studied HA samples were identified by Fourier transform infrared/attenuated total reflectance (FTIR/ATR) spectra and recorded using a Bruker Vertex 70 spectrometer. HA samples were mixed with KBr (approximately 2 mg of sample for 200 mg of KBr) and prepared as pellets. Spectra were collected in the 4000–400 cm^{-1} region with a resolution of 4 cm^{-1}, at room temperature.

CP/MAS ^{13}C-NMR spectroscopy

Cross-polarization magic angle spinning (CP/MAS) ^{13}C-NMR spectra for the solid humic acids samples extracted from peat and lignite, as well as the reference samples of HA and their sodium salts, were obtained using a Bruker Avance 300 equipped with a 4 mm wide-bore MAS probe. Measurement parameters were selected according to the procedure described by Conte et al. [31]. Spectrometer operated at resonance frequency ^{13}C 75.45 MHz and rotation of the samples at 5 kHz. For each sample, 1800 data points were collected. The acquisition time was 20 ms and the recycle delay was 3 s. Spectra were collected at 301 K.

Elemental composition

The bulk elemental composition of humic acids isolated from peat and lignite, as well as HA and their salts, purchased from Sigma-Aldrich, was determined by the use of a CHNS Vario EL Cube instrument, with the use of sulfanilamide as standard.

Thermogravimetry—differential thermal analysis—mass spectroscopy

Thermogravimetry (TG) and differential thermal analysis (DTA) coupled with mass spectroscopy (MS) were used to perform thermal analysis of HA samples and their mixtures with AN. For TG–DTA and coupled MS analyzes, Netzsch STA 449 F3 and Netzsch Aëolos QMS 403 C

were used, respectively. The measurement was performed under synthetic air conditions with a gas flow equal to 30 mL·min^{-1} and with a heating rate equal to 5 K·min^{-1} up to 1100 °C (for HA samples) or 500 °C (for mixture of AN and HA samples). The samples were weighed in the alumina crucible with a pierced lid and the initial sample mass was ~20.00 mg. The mixture of AN and HA, before being weighed in the crucible, was ground in the mortar to homogenize the sample. From the MS analysis, selected mass-to-charge ratios (m/z) were observed and consisted of following signals: 12 (CO, CO_2, HC-fragmentation), 15 (NH_3), 17 (NH_3, H_2O), 18 (H_2O), 36 and 38 (mainly HCl), 44 (CO_2, N_2O), 46 (NO_2), 48 and 64 (SO_2).

Results and discussion

Molecular structure of humic acids

To describe the influence of the molecular structure of humic acids extracted from various raw materials on their thermal stability, as well as on the thermal decomposition of humic acids and ammonium nitrate systems, spectroscopic analysis of these substances was performed. The combination of FTIR/ATR and CP/MAS ^{13}C NMR methods allowed identification of characteristic functional groups, as well as the spatial structure related to the presence of carbon atoms in various molecular fractions.

To account for functional groups that were characteristic for humic structures, we compared FTIR peaks identified for obtained samples with signals for reference substances, which were humic acids and their sodium salts purchased from Sigma Aldrich (Fig. 1). In our interpretation, we also based our assessment on the information collected from other manuscripts. Expectedly, the FTIR spectra for the humic substances (HSs) exhibited characteristic absorption peaks. In general, the wide and intense band at 3400 cm^{-1} is –OH stretching vibrations of the acid, protein, and polysaccharide groups [32, 33]. Peaks at 2950 and 2850 cm^{-1} are characteristic of the symmetric and asymmetric vibrations of –CH_3 and CH_2 in saturated aliphatic chains [34, 35]. Intensive signal at 1710 cm^{-1} can be attributed to asymmetric C=O stretching of –COOH groups [36, 37]. This peak was not detected for sodium salts of humic acids, probably because of the lack of undissociated carboxyl groups for this sample. The band around 1620 cm^{-1} has been assigned to factors that include stretching of C=C of aromatic structures and C=O of amides [38, 39]. Band at about 1220 cm^{-1}, mainly corresponded to the stretching vibrations of C–O structures in aryl ethers and carboxylic acids, but it might be also characteristic of the –OH bending of phenolic units. The peak of approximately 1040 cm^{-1}, which was particularly intensive for HA extracted from lignite and a sample of
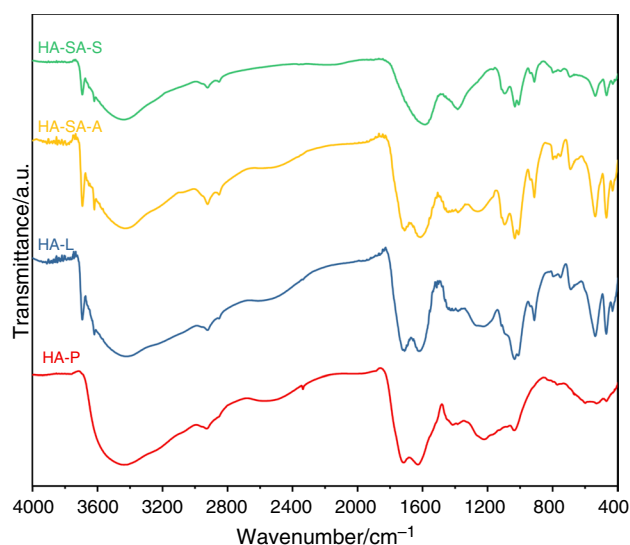
Fig. 1 FTIR spectra of humic acids extracted from peat (HA-P), lignite (HA-L) and of reference samples purchased from Sigma Aldrich (HA-SA-A and HA-SA-S)
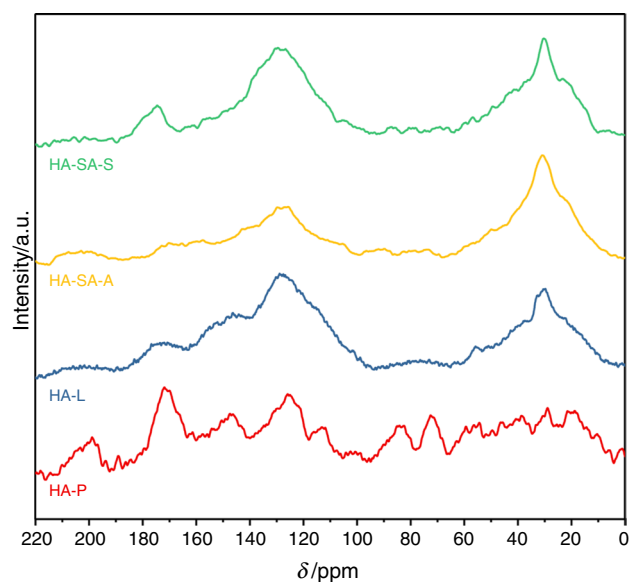
Fig. 2 CP/MAS ^{13}C NMR spectra of humic acids extracted from peat (HA-P), lignite (HA-L) and of reference samples purchased from Sigma Aldrich (HA-SA-A and HA-SA-S)

humic acids purchased from Sigma, as well as peaks below 1000 cm^{-1} (especially at 530 and 470 cm^{-1}) are probably associated with Si–O stretching in mineral substances (e.g. kaolinite) as well as SiO–S and S–S vibrations [35–37].

The CP/MAS ^{13}C NMR spectra in Fig. 2 provide a representation of the carbon content in various bindings in the chemical structure of the humic samples. Functionalities associated with the chemical shift in the three main ranges

(0–110; 110–160 and 160–220 ppm) are assigned, respectively, as aliphatic carbons, aromatic carbons and carboxyl/carbonyl carbons [40]. Additionally, according to Fernandes et al. [27], results of the cross-polarization and magic spinning techniques for ^{13}C nuclear magnetic resonance allow for a better resolved spectra. Therefore, it is possible to divide the resonance region of aliphatic carbon into 2 subareas, which were attributed to saturated non-substituted carbons in aliphatic chains (alkyl C for 0–50 ppm) and aliphatic carbons bound to oxygen or nitrogen (O-alkyl C for 50–100 ppm). For carbonyl/carboxyl carbons, the resonance region can be divided into subareas associated with carboxylic acid, ester and amide (160–190 ppm), and carbonyl carbons of aldehydes and ketones (190–220 ppm) [10, 41, 42].

Presented spectra exhibit three main signals peaking at 30, 128 and 173 ppm for all analyzed samples. According to Adani et al. [42] the first peak may be assigned to aliphatic, methylene carbon in long chains and terminal methyl groups. The second one is characteristic for the presence of aromatic carbon substituted by a carboxyl or carboxymethyl group and the aromatic carbon that is in meta position to the nitrogen or oxygen substituent. The last peak (173 ppm) may be assigned to carbon in carboxylic acids, esters and amides. Moreover, at the spectra of humic acids extracted from peat, additional signals, peaking at 56, 73 and 150 ppm, were observed. The presence of these peaks indicates the participation of lignin residues and peptide structures (56 ppm), ring polysaccharides such as cellulose (73 ppm) and carbons bound to phenolic groups (150 ppm) [35, 41].

Based on relative areas of the bands for the spectra, the carbon distribution is reported and obtained results are presented in Table 1. For presented results, ratios of aromatic to aliphatic carbon and alkyl to O-alkyl were defined. Moreover, according to Zhang et al. [43], ratios of hydrophobic to hydrophilic carbon for each sample were calculated. Hydrophobic carbons were defined as a sum of alkyl and aromatic C, while hydrophilic C as a sum of O-alkyl, carbonyl and carboxyl carbon. The ratio of aromatic to aliphatic carbon may be used for the assessment of the degree of humification of the HA structure. A higher percentage of aliphatic C and a lower amount of aromatic C were characteristic for the HA extracted from the peat. The ratio of aromatic to aliphatic carbon for this sample, as well as for reference samples, was less than 1 and means a relatively low degree of humification compared to HA obtained from lignite. This was also confirmed by ^{13}C CP/MAS NMR spectra, which suggested the presence of cellulose and lignin residues in humic acids extracted from peat, which are characteristic of samples at the initial stage of humic transformation [44]. According to Xu et al. [45], the ratio of alkyl C to O-alkyl C may be considered as an index of the degree of decomposition of humic acids. The lowest

Table 1 The carbon atoms distribution by CP/MAS ^{13}C NMR in humic acids extracted from peat, lignite and for reference samples

Sample	Alkyl C (0–50 ppm)/%	O-alkyl C (50–110 ppm)/%	Aromatic C (110–160 ppm)/%	Carboxyl C (160–190 ppm)/%	Carbonyl C (190–220 ppm)/%	Aliphatic C/%	Aromatic/aliphatic C	Alkyl/O-alkyl C	Hydrophobic/hydrophilic C
HA-P	25.4	21.6	30.6	14.4	8.0	47.0	0.66	1.18	1.27
HA-L	27.8	12.2	45.4	10.3	4.3	40.0	1.14	2.28	2.73
HA-SA-A	34.5	16.8	31.0	9.7	8.0	51.3	0.61	2.05	1.90
HA-SA-S	32.0	14.0	40.8	9.4	3.8	46.0	0.89	2.29	2.68

Table 2 Elemental composition of humic acids samples

| Sample	C/%	H/%	N/%	S/%
HA-P	40.1	4.2	2.5	2.2
HA-L	40.0	3.6	0.8	1.8
HA-SA-A	36.2	3.6	0.8	0.5
HA-SA-S	36.0	3.8	0.8	0.4

value of this parameter, of four samples analyzed, was observed for humic acids isolated from peat (1.18) and for other samples that value was higher than 2. The high percentage of alkyl carbon bonded to oxygen and nitrogen indicates a high reactivity of humic acids extracted from peat (HA-P). O-alkyl C is considered to be a stable form of carbon in the HA structure [43]. However, Liu et al. [46] concluded that the O-alkyl form of carbon is mainly composed of cellulose and hemicellulose, which can be exposed to microbiological decomposition. Therefore, based on FTIR and, above all, ^{13}C CP/MAS NMR spectra, it can be concluded that the use in the extraction process carbon raw material with a low degree of carbonization (such as peat) allows the obtainment of humic acids with a higher percentage of hydrophilic carbon, defined as form bonded with heteroatoms, that are characteristic of humic substances with lower transformation degree.

To describe the differences in the elemental composition between humic acids isolated from various raw materials, the contents of carbon (C), hydrogen (H), nitrogen (N) and sulfur (S) were determined, and the results were presented in Table 2. From each sample tested, the determination of the content of the given element was made in triplicate and the arithmetic mean was taken as the final result. Based on the results presented below, it can be concluded that samples obtained in our laboratory from peat (HA-P) and lignite (HA-L) were characterized by the higher carbon content, compared to reference samples (HA-SA-A and HA-SA-S). Furthermore, these samples were also characterized by a higher sulfur content, which may be related to the presence of this element in the raw materials from which they were isolated.

TG–DTA-MS results

Analysis of the extracted HA

The thermal analysis of a sample containing humic acids extracted from peat raw material (HA-P) is shown in Fig. 3a. The DTA and TG signals indicate multistage decomposition; therefore, Table 3 contains proposed following stages with the most likely ongoing thermal processes. The combustion process was accompanied by exothermic effects, with maxima observed at 333, 454, 520, 573 and 732 °C. The total heat effect was 29 kJ·g^{-1} with a final mass loss of 88%. The main combustion process of the sample occurred in the temperature range of 177–613 °C, where the mass loss was 70% and was preceded by a mass loss of 9%. The thermal decomposition of the sample of humic acids extracted from lignite (HA-L) is shown in Fig. 3b. Up to a temperature of 174 °C, the mass loss was around 7%. The combustion stage started above 200 °C and was assisted by an exothermic effect of 27 kJ g^{-1}. The cumulative mass loss up to 616 °C, due to the intense combustion of the sample, has been equal to 67%. Thermal analysis of a reference sample of humic acids (HA-SA-A) is shown in Fig. 3c. The initial mass loss to 205 °C reached 8%. The combustion of the sample began slowly and continued almost monotonically to a temperature of 580 °C. During the combustion, 22 kJ·g^{-1} of energy was released and the mass loss was registered as 62%. The exothermic maxima were reached at 476 and 508 °C. Above 580 °C, a gradual afterburn of the sample began, lasting up to nearly 1000 °C. The total mass loss was 73%. The thermal decomposition of the reference sample, which contained sodium salts of humic acids (HA-SA-S), is shown in Fig. 3d. The TG–DTA curve suggests a very complex combustion process of the test sample. Up to a temperature of 201 °C, a loss of 16 mass% is evident. Then, in the temperature range of 201–652 °C, several smaller mass effects are visible, with a total mass loss of 27%. In the temperature range of 652–818 °C, the last most rapid combustion stage occurs, with a mass loss of 27%. During the decomposition, exothermic maxima were reached at temperatures of 301, 406, 456 and 661 °C, with a total heat release of 39 kJ g^{-1}.

(a)

(b)

(c)

(d)
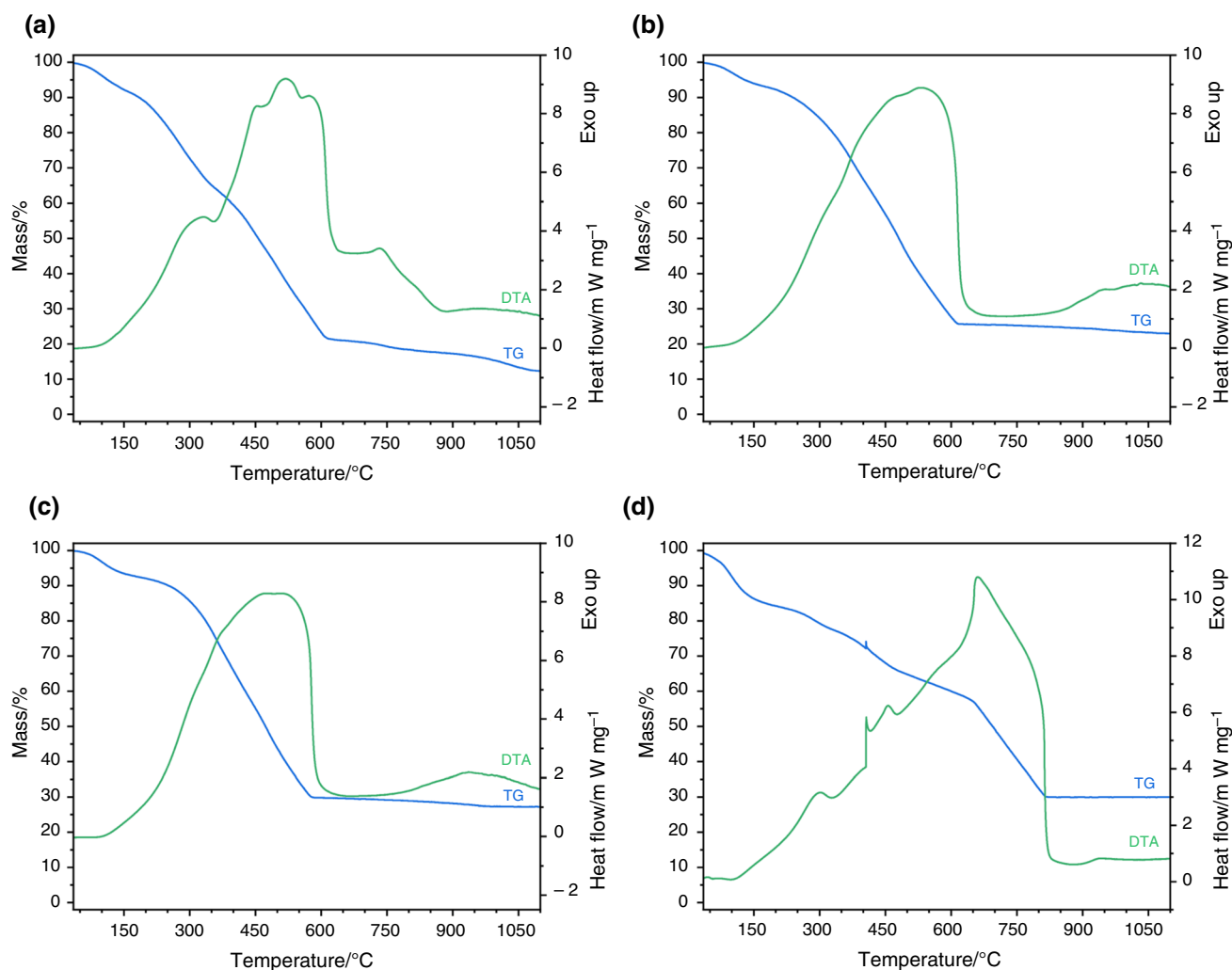
Fig. 3 Thermogravimetric (TG) and differential thermal analysis (DTA) data collected during heating of the samples up to 1100 °C with a heating rate 5 K·min^{-1} and in air atmosphere. **a** HA-P, **b** HA-L, **c** HA-SA-A, **d** HA-SA-S

Table 3 Mass loss during thermal decomposition of HA samples with the proposal of possible processes occurring in a given temperature range

Sample	Δm_1		Δm_2		Δm_3		Δm_4		Residual mass
	mass%	°C	mass%	°C	mass%	°C	mass%	°C	mass%
HA-P	9	Up to 177	27	177–362	43	362–613	9	613–1090	12
HA-L	7	Up to 174	31	174–426	36	426–616	3	616–1073	23
HA-SA-A	8	Up to 205	34	205–436	28	436–580	3	580–1006	27
HA-SA-S	16	Up to 201	27	201–652	27	652–818	–	–	31
Suggest thermal process	Dehydration		Decomposition of unsubstituted aliphatic chains and unbranched aliphatic chains containing heteroatoms		Simultaneous decomposition of branched chains and aromatic structures, as well as heteroatom groups		Decomposition of mineral matter, mainly carbonate impurities		Residue from the combustion process, mainly silicates, sulfates, and oxides
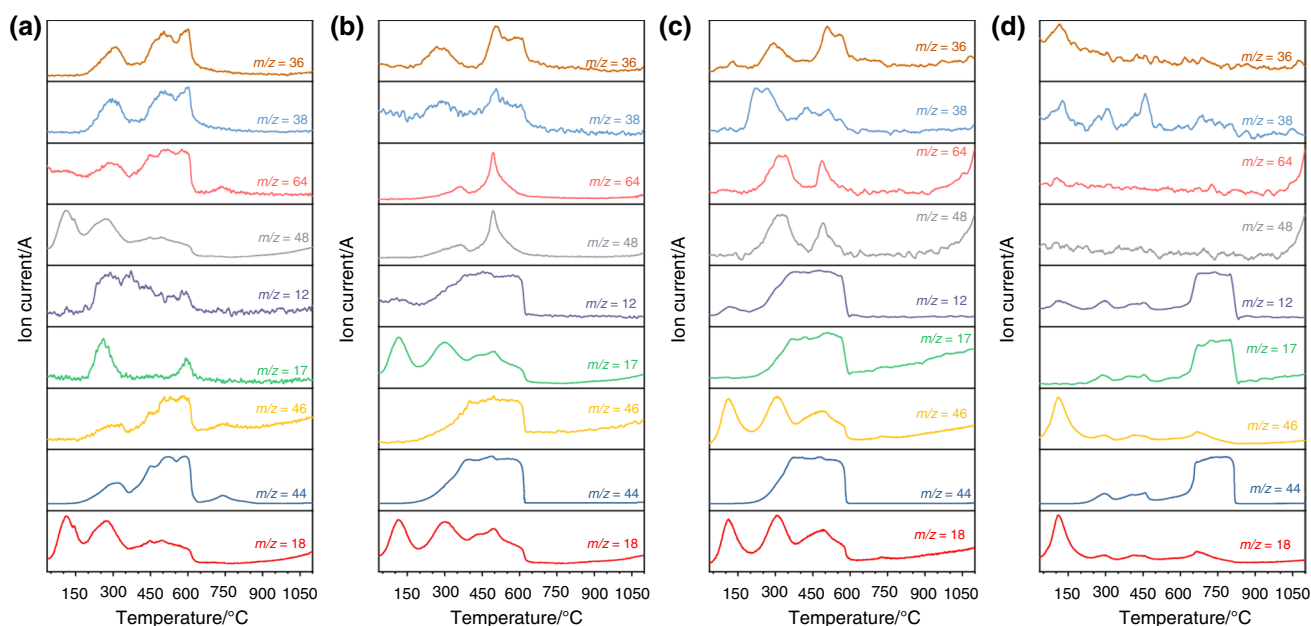
Fig. 4 Mass Spectroscopy (MS) results for the thermal decomposition of HA samples. $T_{max} = 1100$ °C, $\beta = 5$ K min^{-1}, air atmosphere. **a** HA-P, **b** HA-L, **c** HA-SA-A, **d** HA-SA-S

Analysis of the gas phase (Fig. 4a–d) indicates the appearance of $m/z = 17$ and $m/z = 18$ signals, which are identified as signals for H_2O molecules. The presence of H_2O-identical signals at higher temperatures was caused by the combustion process of total organic matter in the air atmosphere to CO_2 and H_2O. Arenillas et al. [47] suggested that H_2O below 300 °C may also reflect the decomposition of oxygen-rich functional groups, especially hydroxyl groups. Signals that confirm the combustion of organic matter are visualized by peaks $m/z = 12$ and $m/z = 44$, which mainly correspond to CO_2. At high temperatures, when the peak signal $m/z = 44$ is clear and the signal $m/z = 12$ is invisible, the signal $m/z = 44$ indicates the decomposition of carbonate minerals into CO_2. MS analysis also identified signals of $m/z = 46$, suggesting NO_2 release, which most likely comes from the high nitrogen group present in the sample. HA-P and HA-L samples present quite similar intensity characteristics at both m/z 36 and m/z 38 ratios. Whereas for the reference samples, the m/z 36 and m/z 38 curves present different variations in recorded intensity. Thus, it can be inferred that in the extracted HA samples m/z 36 and m/z 38 ratios will mainly characterize the presence of chlorides in the gas phase. These may be from impurities in the sample and could also be the result of their introduction into the sample in the form of HCl during the preparation stage. Differences observed within referenced samples suggest that during analysis there were also fragments of evaporating or sublimating organic matter in the gas phase. $M/z = 48$ and 64 indicate the appearance of sulfur oxides, which most likely reflect sulfur contamination of the sample.

The first step in the decomposition of HA samples is related to the release of free water, which is evident mainly by the appearance of H_2O indicating signals during MS analysis. Depending on the raw material of the sample that was extracted, these values varied. Some scientists indicate that, in this temperature range, it is also possible to volatilize smaller organic structures and break down aliphatic chains into smaller ones [48]. The next stage is related to the decomposition of organic matter. This process is consistent with the initial combustion of aliphatic straight chains. Temperatures at the beginning of this combustion suggest that their values have been affected by the amount of carbonyl and carboxyl groups. It is in agreement with the results of the Boguta et al. [49] research. Their research has shown that the decomposition of the organic structure is mainly related to the decomposition of carboxyl groups below 430 °C. Also, Dell'Abate et al. [50], suggested that, in the range 200–350 °C, the degradation of carboxylic groups mainly occurs. Combustion was fastest in the HA-P sample, where, together with a high proportion of aliphatic groups, it also has the highest proportion of groups determining the high reactivity (Table 1). However, the faster decomposition of the HA-P sample can also be explained by the lower degree of humification—HA extracted from peat, in relation to HA samples extracted from lignite. With a low degree of humification, the amount of carbon groups with heteroatoms increases. From the MS analyses, it can be seen that in the first stage of decomposition, SO_2 and NO_2 maxima are reached fastest for the HA-P samples; therefore, it can be concluded that, within this range of temperatures,

short carbon chains rich in heteroatom groups are also decomposed.

A further mass step is most likely related to burning of remaining longer aliphatic chain fragments, present in the HA structure, and aromatic groups. According to the MS analysis, in addition to CO_2, SO_2 and NO_2 were detected among evacuated gaseous products. Their intensity was much higher than the one that was observed in the initial combustion phase of the HA sample. Therefore, it is concluded that the decomposition of carbon structures rich in heteroatoms does not occur exclusively in one strict temperature range and is determined by the distribution of these atoms in groups that build the HA structure. The literature suggests that, within 375–800 °C, the decomposition of long-chain hydrocarbons, N-compounds, and the degradation of the aromatic structure were observed [51]. The HA-L and HA-SA-A curves show a very similar decomposition pattern. However, the HA-L TG curve decreased slightly slower. The two substance groups differ mainly in the proportion of aromatic groups; hence, it may be concluded that their proportion will determine the final combustion temperature of samples with a similar combustion mechanism. The final stage of the observed combustion process is mainly related to the thermal decomposition of some mineral substances (majorly carbonates) present in the studied samples [27]. There are small visible peaks of CO_2 in the MS analysis. Above 1000 °C, increasing intensity of SO_2 signals was noticed, which is very

probably related to the decomposition of sulfates, another mineral impurities of the raw carbon material.

Each sample was characterized by a different mineral residue. These differences are caused by the variety of starting material from which HA was extracted. Surprisingly, the mass residue was obtained after combustion of HA-P. HA-P are characterized by the lowest degree of humification; hence, the expected result was to obtain the highest mass residue amongst studied samples. However, HA-P was very rich in mineral impurities in the form of carbonates, which were decomposed during the experiment, resulting in the lowest value of the residual mass. Low mass losses in the other samples suggest that mineral impurities, in the form of carbonates, were much lower and the main residue is likely to be comprised of silicates. The thermal decomposition path of the HA-SA-S sample was also intriguing, presenting a completely different decomposition process. This type of the thermal decomposition pattern of HA samples is encountered in the literature. According to Kara et al. [52], this is due to the significant proportion of mineral impurities in the form of clays (aluminates, silicates, aluminosilicates). During combustion, they form an impermeable layer that prevents the organic matter from burning. Above a certain temperature, this layer breaks down or increases in porosity, as gaseous products of combustion of the organic matter diffuse after the phase transition of the clay, resulting in a steady decrease in mass.

Table 4 The characteristic parameters provided by the thermal analysis of pure AN and its mixtures with HA extracted from a different source

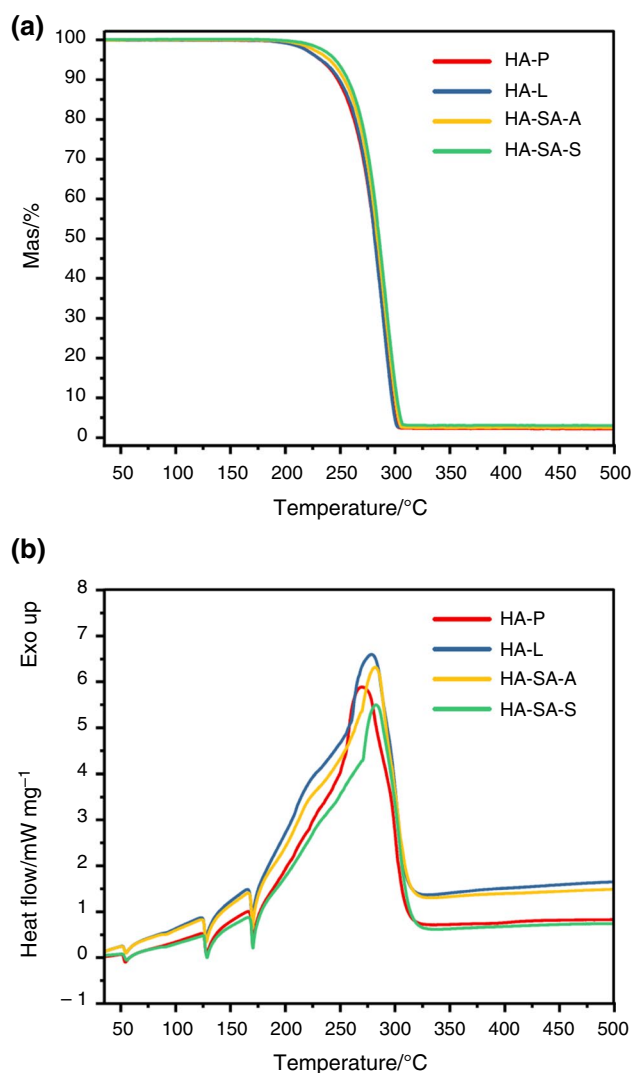| HA type in the mixture with AN	HA content/mass%	Temperature of phase transition /°C				Start of decomp. /°C	Exotherm maximum /°C			End of decomp. /°C	Heat evolved during decomp. /J g^{-1} AN
		IV→II	III→II	II→I	Melting		I	II	III		
AN [55]	–	51	84	124	167	235	283	–	–	297	1311
HA-P	0.1	51	–	125	168	238	287	–	–	304	1921
	0.5	51	–	126	168	226	270	–	–	303	2084
	2.0	52	85	126	168	203	261	274	–	295	2959
	10.0	52	86	125	165	180	234	263	275	291	5127
HA-L	0.1	52	–	126	169	240	281	289	–	309	1449
	0.5	52	–	125	168	229	279	–	–	302	1975
	2.0	53	88	125	168	212	273	285	–	299	2221
	10.0	53	90	121	161	173	228	245	–	273	5660
HA-SA-A	0.1	52	–	126	169	240	281	293	–	308	1333
	0.5	52	87	125	168	235	282	–	–	306	1699
	2.0	52	87	125	167	215	273	280	–	295	2315
	10.0	52	–	122	161	193	242	267	–	281	4365
HA-SA-S	0.1	52	–	126	168	240	285	–	–	308	1175
	0.5	52	–	126	169	239	283	–	–	307	1593
	2.0	52	–	126	168	232	277	286	–	294	1383
	10.0	52	–	125	158	191	277	–	–	289	4885

(a)

(b)
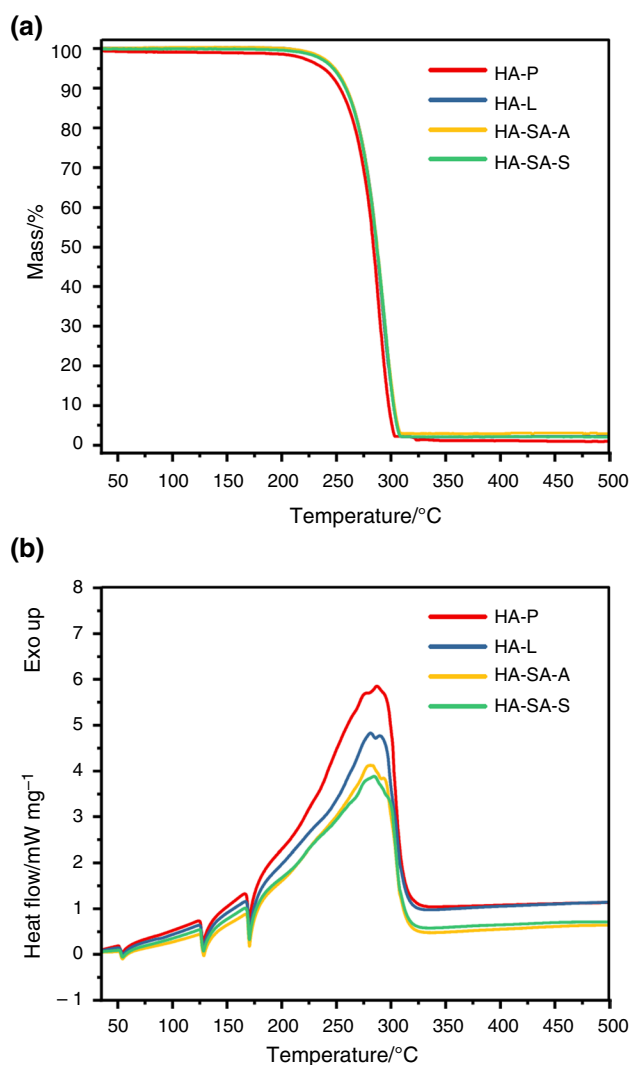
Fig. 5 Thermal decomposition of mixture of AN and 0.1 mass% HA from different sources up to 500 °C with a heating rate of 5 K min^{-1} and in air atmosphere. **a** TG, **b** DTA
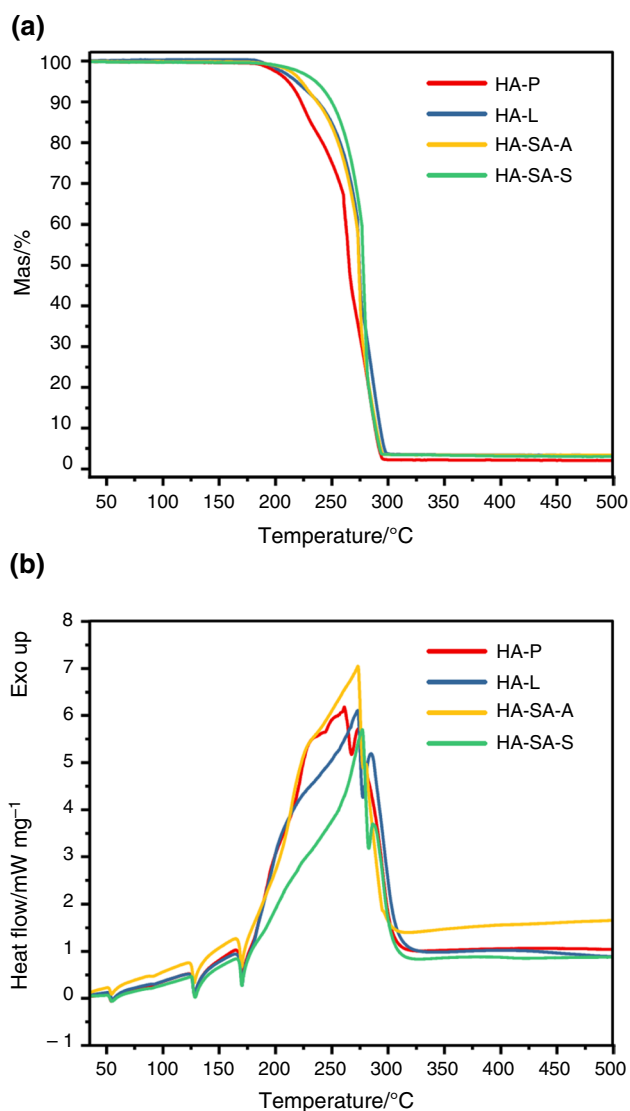
(a)

(b)

Fig. 6 Thermal decomposition of mixture of AN and 0.5 mass% HA from different sources up to 500 °C with a heating rate of 5 K min^{-1} and in air atmosphere. **a** TG, **b** DTA

Analysis of the HA and AN mixture

The characteristic parameters determining the decomposition of ammonium nitrate mixtures with humic acids of different sources are collected in Table 4. Figures 5a–b and 6a–b present TG-DTA curves for the investigated mixtures with 0.1 mass% and 0.5 mass% of different HAs samples, respectively. TG-DTA curves in both cases present similar thermal decomposition pathways, and visible changes are seen in the heat evolved during the exothermic decomposition of composition. The start of the decomposition temperatures for the mixtures mentioned above are very close to the thermal stability parameter of pure AN and varied around
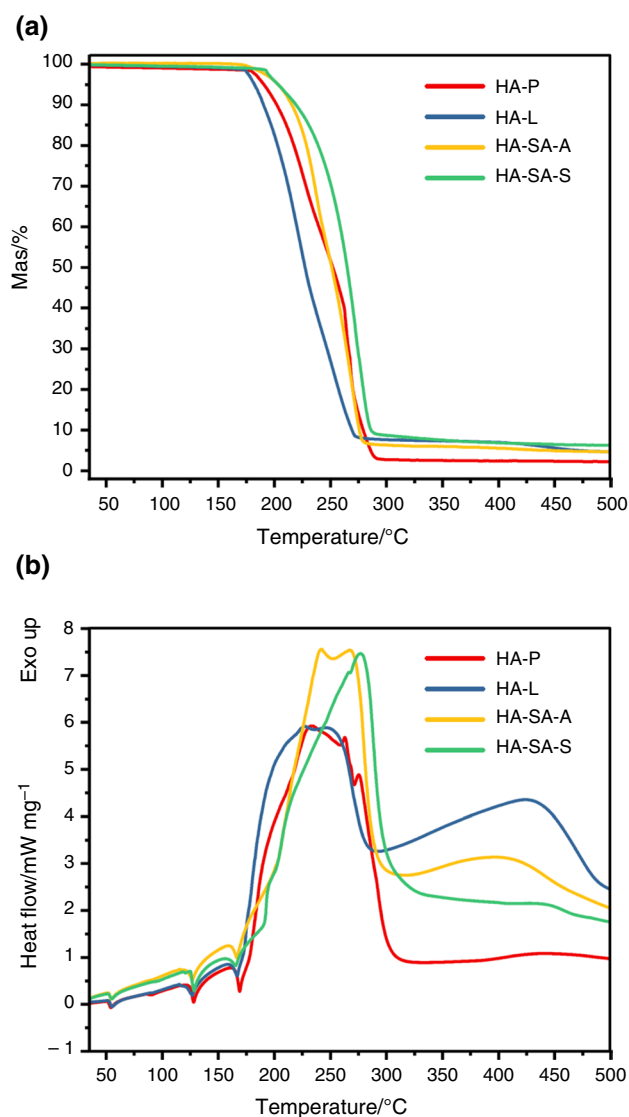
238–240 °C. In the system with 0.5 mass% of HA-P and HA-L, little acceleration has been observed, with a 6–9 °C shift compared to pure AN. With the increasing HA content in the mixture, visible catalysis is existing. Figures 7a–b and 8a–b show TG–DTA results for the 2.0 and 10.0 mass% of HA systems, respectively. TG curves clearly show that the multistep decomposition occurs, which also confirmed DTA analysis by distinguishing multiple exothermal maxima. For systems of 2.0 and 10.0 mass% Has, the reactions associated with the mixture decomposition were significantly shifted towards lower temperatures. In the case of 10.0 mass% HA,
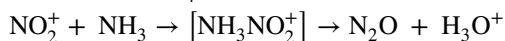
(a)

(b)

Fig. 7 Thermal decomposition of mixture of AN and 2.0 mass% HA from different sources up to 500 °C with a heating rate of 5 K min^{-1} and in air atmosphere. **a** TG, **b** DTA

(a)

(b)

Fig. 8 Thermal decomposition of mixture of AN and 10.0 mass% HA from different sources up to 500 °C with a heating rate of 5 K min^{-1} and in air atmosphere. **a** TG, **b** DTA

the start of thermal decomposition has been estimated below 200 °C.

The process of the exothermic decomposition in studied samples was dependent on the mass ratio of the introduced additive. In the 0.1 mass%, 0.5 mass% and 2 mass% systems, the temperature of the exothermic decomposition beginning decreased according to the order HA-SA-S > HA-SA-A > HA-L > HA-P. However, the proportion of carboxyl groups in the HA samples increased with an inverse relationship. It may be very possible that the observed initial thermal stability was correlated by the appearance of Lewis acid molecules (for example, H_3O^+) formed by dissociation of carboxyl groups. At this time, catalysis of the decomposition of ammonium nitrate

was observed, according to a molecular mechanism described by the following reaction pathway [53, 54].

$$NH_4NO_3 \leftrightarrow NH_3 + HNO_3$$

$$HNO_3 + A \leftrightarrow H_2ONO_2^+ \rightarrow NO_2^+ + H_2O$$

where A = NH_4^+, H_3O^+, etc.

$$NO_2^+ + NH_3 \rightarrow [NH_3NO_2^+] \rightarrow N_2O + H_3O^+$$

A possible catalysis, related to the dissociation of Lewis acid-like molecules from the introduced HA, can be confirmed by results of the MS analysis (Fig. 9). At temperatures close to the initial thermal decomposition temperature of tested mixtures, an increased generation

Fig. 9 Progress in the thermal decomposition of the AN mixture with HA samples (10.0 mass% HA), supported by MS signals correlated with the main gaseous products of the ionic mechanism of decomposition of the AN ($m/z = 44$, N_2O and $m/z = 18$, H_2O)
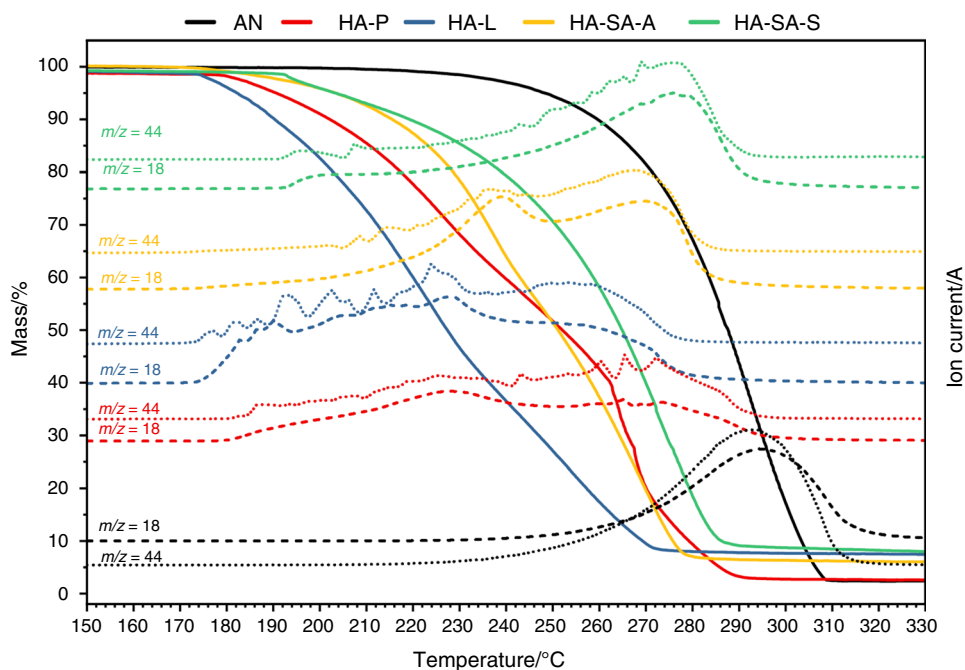
of decomposition products of ammonium nitrate (N_2O and H_2O) was observed. In mixtures with the most reactive HA and with the highest proportion of functional groups, this effect was observed most at lowest temperatures.

Moreover, the structure, carbon skeleton of the organic matter extracted from the HA source and the proportion of individual functional groups forming the HA sample were also significant factors. It is noticeable that the thermal decomposition was determined by the ratio of aromatic to aliphatic carbon and the ratio of hydrophobic to hydrophilic carbon, both of which describe the reactivity of HA. Samples with similar values were decomposed in a similar pattern or, more precisely, following a very similar combustion mechanism. In all cases, the addition of HA to ammonium nitrate in amounts of 10.0 and 2.0 mass% caused a significant acceleration of the decomposition process of AN and combustion of the introduced organic matter.

For HA-L, between 300 and 500 °C, a slight decrease in mass is observed of less than 2%. For the rest, the mass loss above 300 °C was negligible. This effect is probably caused by the decomposition of compounds with aromatic groups, whose ratio to aliphatic groups in HA-L was the highest. During heating to 170 °C, phase transformations typical of ammonium nitrate are observed. Only the melting point shifted towards lower temperatures with an increase in the proportion of HA in the mixture. The amount of heat generated during the decomposition of the mixtures was significantly higher in systems containing 10 and 2 mass% HA in comparison to the energy of the decomposition of pure ammonium nitrate. Furthermore, the progress of thermal decomposition of ammonium nitrate comprised in studied

samples was apparently determined by the reactivity and thermal stability of introduced humic acids.

HA-SA-S, with the highest proportion of mineral residues, low reactivity in relation to HA-P or HA-SA-A and the lowest proportion of carboxyl and carbonyl groups, followed a standard pattern in thermal decomposition similar to that of pure ammonium nitrate. However, a difference in the form of a decrease in the start temperature of the decomposition was only apparent when the amount of HA-SA-S in the sample was 2 mass% or more. Other samples of HA were characterized with higher proportions of reactive groups as well as the number of connections to heteroatoms. This fact had an apparent effect on the decomposition reactions of ammonium nitrate, resulting in a significant decrease in the start temperature of the thermal decomposition and an increase in the amount of heat evolved.

Conclusions

In this work, a comprehensive analysis of humic acids extracted from various raw materials and assessment of their influence on the thermal decomposition of ammonium nitrate were performed. Generally, comparison of isolated humic acids with reference samples showed the presence of structures that are characteristic for these macromolecular substances, such as aliphatic chains, aromatic rings, carboxyl and phenolic units, etc. Elemental analysis of humic acids samples tested showed a higher content of carbon and sulfur for HA extracted from peat and lignite, compared to the results for the reference

samples. Spectroscopic methods for the determination of the structure of humic acids showed significant differences between the HA extracted from two types of raw material. Humic acids isolated from peat, in reference to humic acids extracted from lignite, were characterized by a higher amount of hydrophilic carbon, which is defined as carbon atoms linked with heteroatoms. That sample also had a higher amount of aliphatic carbon. CP/MAS ^{13}C NMR spectra for the HA-P sample showed signals that are characteristic of peptides, polysaccharides, and lignin residues, indicating a lower degree of humic transformation, compared to the sample extracted from lignite. The difference in the degree of humification for extracted samples is also evidenced by a higher hydrophilic to hydrophobic carbon ratio for the HA-P sample. Qualitative analysis of the humic sample extracted from peat also showed a higher percentage of alkyl C bounded with nitrogen and oxygen atoms, compared to other tested samples. Moreover, it may be concluded that these structures in studied HA have a significant impact on the thermal decomposition characteristic of these samples as well as on the ammonium nitrate—HA systems. That was especially seen when the organic structure was rich in carboxylic and/or hydroxylic functional groups. Thermal analysis of tested samples revealed the presence of mass loss signals above 600 °C, which can be assigned to the presence of mineral contaminations in HA samples. It was further confirmed by obtained FTIR spectra and by MS analysis with signals for carbonates, which occur after organic matter combustion.

From the present results, one could conclude that a small addition of HA (less than 0.5 mass%) did not significantly affect the decomposition mechanism of ammonium nitrate. Furthermore, when the HA sample was comprised of its sodium salt, the thermal stability of its mixture with ammonium nitrate has not been worsened. Taking into account the analysis of the elemental composition of humic acids (about 40% of carbon), it can be concluded that the addition of 0.2 mass% of carbon from HA should not have a significant, negative impact on the thermal decomposition of ammonium nitrate. Therefore, the introduction of small doses of HA (maximum of 0.5 mass%) into ammonium nitrate-based fertilizers should be safe and may have a biostimulant effect on the plants.

Author contributions DN, MB contributed to Conceptualization; KM, MB, MH-M, MK, JZ contributed to Methodology; DN, MH-M, MK contributed to Formal analysis and investigation; DN, MB, KMa contributed to Writing—original draft preparation; MH-M, MK, JZ contributed to Writing—review and editing; MH-M contributed to Funding acquisition; JH contributed to Resources and Supervision. All authors have read and agreed to the published version of the manuscript.

Declarations

References

1. Barłóg P, Grzebisz W, Łukowiak R. Fertilizers and fertilization strategies mitigating soil factors constraining efficiency of nitrogen in plant production. Plants. 2022;11:1855. https://doi.org/10.3390/plants11141855.

2. Barłóg P, Łukowiak R, Grzebisz W. Predicting the content of soil mineral nitrogen based on the content of calcium chloride-extractable nutrients. J Plant Nutr Soil Sci. 2017;180:624–35. https://doi.org/10.1002/jpln.201700136.

3. Nieder R, Benbi DK, Scherer HW. Fixation and defixation of ammonium in soils: a review. Biol Fertil Soils. 2011;47:1–14. https://doi.org/10.1007/s00374-010-0506-4.

4. Murphy BW, Murphy BW. Impact of soil organic matter on soil properties—a review with emphasis on Australian soils. Soil Res. 2015;53:605–35. https://doi.org/10.1071/SR14246.

5. Khaled H, Fawy H. Effect of different Levels of humic acids on the nutrient content, plant growth, and soil properties under conditions of salinity. Soil Water Res. 2011;6:21–9. https://doi.org/10.17221/4/2010-SWR.

6. de Oliveira KS, Mendes MC, Ilibrante GA, Antoniazzi N, Stadler AJ, Antoniazzi AP. Export of N, P and K in barley subjected to fertilizer doses formulated with and without humic substance at sowing. Acta Sci Agron. 2019. https://doi.org/10.4025/actasciagron.v41i1.42690.

7. Martins JDL, Soratto RP, Fernandes AM. The effect of humic substances and phosphate fertilizer on growth and nutrient uptake of the potato. Commun Soil Sci Plant Anal. 2020;51:1525–44. https://doi.org/10.1080/00103624.2020.1781154.

8. Saruhan V, Kusvuran A, Üniversitesi ÇK. The effect of different humic acid fertilization on yield and yield components performances of common millet (*Panicum miliaceum* L.). Sci Res Essays. 2011;6:3663–9.

9. Pavlovich LB, Strakhov VM. Effect of humic fertilizers from brown coal on the mineral composition of vegetable crops. Solid Fuel Chem. 2018;52:206–10. https://doi.org/10.3103/S0361521918030084.

10. Huculak-Mączka M, Hoffmann J, Hoffmann K. Evaluation of the possibilities of using humic acids obtained from lignite in the production of commercial fertilizers. J Soils Sediments. 2018;18:2868–80. https://doi.org/10.1007/s11368-017-1907-x.

11. Erro J, Urrutia O, Baigorri R, Fuentes M, Zamarreño AM, Garcia-Mina JM. Incorporation of humic-derived active molecules into compound NPK granulated fertilizers: main technical difficulties and potential solutions. Chem Biol Technol Agric. 2016;3:1–15. https://doi.org/10.1186/s40538-016-0071-7.

12. Gorbovskiy K, Kazakov A, Norov A, Malyavin A, Mikhaylichenko A. Properties of complex ammonium nitrate-based fertilizers depending on the degree of phosphoric acid ammoniation. Int J Ind Chem. 2017;8:315–27. https://doi.org/10.1007/s40090-017-0121-4.

13. Sivaraman S, Varadharajan S. Investigative consequence analysis: a case study research of beirut explosion accident. J Loss Prev Process Ind. 2021;69:104387. https://doi.org/10.1016/j.jlp.2020.104387.

14. Baraza X, Pey A, Giménez J. The self-sustaining decomposition of ammonium nitrate fertiliser: case study, Escombreras valley, Spain. J Hazard Mater. 2020;387:121674. https://doi.org/10.1016/j.jhazmat.2019.121674.

15. Xu ZX, Cheng JHJ, Wang Q, Cheng JHJ, Hu X. The influence of dissociation reaction on ammonium nitrate thermal decomposition reaction. J Therm Anal Calorim. 2019;136:1415–24. https://doi.org/10.1007/s10973-018-7808-4.

16. Xia R, Wang J, Han Z, Li Z, Mannan MS, Wilhite B. Mechanism study of ammonium nitrate decomposition with chloride impurity using experimental and molecular simulation approach. J Hazard Mater. 2019;378:120585.

17. Han Z, Sachdeva S, Papadaki MI, Mannan S. Effects of inhibitor and promoter mixtures on ammonium nitrate fertilizer explosion hazards. Thermochim Acta. 2016;624:69–75. https://doi.org/10.1016/j.tca.2015.12.005.

18. Oxley JC, Smith JL, Rogers E, Yu M. Ammonium nitrate: thermal stability and explosivity modifiers. Thermochim Acta. 2002;384:23–45. https://doi.org/10.1016/S0040-6031(01)00775-4.

19. Sun J, Sun Z, Wang Q, Ding H, Wang T, Jiang C. Catalytic effects of inorganic acids on the decomposition of ammonium nitrate. J Hazard Mater. 2005;127:204–10. https://doi.org/10.1016/j.jhazmat.2005.07.028.

20. Hoffmann J, Kaniewski M, Nieweś D, Hoffmann K. Selected magnesium compounds as possible inhibitors of ammonium nitrate decomposition. Pol J Chem Technol. 2020;22:1–8. https://doi.org/10.2478/pjct-2020-0011.

21. Popławski D, Hoffmann J, Hoffmann K. Effect of carbonate minerals on the thermal stability of fertilisers containing ammonium nitrate. J Therm Anal Calorim. 2016;124:1561–74. https://doi.org/10.2478/pjct-2020-0011.

22. Menicacci E, Rotureau P, Fayet G, Adamo C. Toward the Mechanistic understanding of the additives' role on ammonium nitrate decomposition: calcium carbonate and calcium sulfate as case studies. ACS Omega. 2020;5:5034–40. https://doi.org/10.1021/acsomega.9b03964.

23. Orlov DS. Humic substances of soils and general theory of humification. Boca Raton: CRC Press; 2020.

24. Rotaru A, Nicolaescu I, Rotaru P, Neaga C. Thermal characterization of humic acids and other components of raw coal. J Therm Anal Calorim. 2008;92:297–300. https://doi.org/10.1007/s10973-007-8816-y.

25. Scaccia S. TG–FTIR and kinetics of devolatilization of Sulcis coal. J Anal Appl Pyrolysis. 2013;104:95–102. https://doi.org/10.1016/j.jaap.2013.09.002.

26. Song H, Liu G, Zhang J, Wu J. Pyrolysis characteristics and kinetics of low rank coals by TG-FTIR method. Fuel Process Technol. 2017;156:454–60. https://doi.org/10.1016/j.fuproc.2016.10.008.

27. Shi L, Liu Q, Guo X, Wu W, Liu Z. Pyrolysis behavior and bonding information of coal—a TGA study. Fuel Process Technol. 2013;108:125–32. https://doi.org/10.1016/j.fuproc.2012.06.023.

28. Kolokassidou C, Pashalidis I, Costa CN, Efstathiou AM, Buckau G. Thermal stability of solid and aqueous solutions of humic acid. Thermochim Acta. 2007;454:78–83. https://doi.org/10.1016/j.tca.2006.12.022.

29. Li Y, Zhang Y, Chang L, Zi C, Liang G, Zhang D, et al. Analyses on thermal stability of lignites and its derived humic acids. Ind Eng Chem Res. 2020;60(17):6298–305. https://doi.org/10.1080/15567036.2020.1810828.

30. Trubetskaya OE, Trubetskoj OA, Voyard G, Richard C. Determination of hydrophobicity and optical properties of soil humic acids isolated by different methods. J Geochem Explor. 2013;132:84–9. https://doi.org/10.1016/j.gexplo.2013.06.004.

31. Conte P, Spaccini R, Piccolo A. Advanced CPMAS-13C NMR techniques for molecular characterization of size-separated fractions from a soil humic acid. Anal Bioanal Chem. 2006;386:382–90. https://doi.org/10.1016/10.1007/s00216-006-0637-5.

32. Romarís-Hortas V, Moreda-Piñeiro A, Bermejo-Barrera P. Application of microwave energy to speed up the alkaline extraction of humic and fulvic acids from marine sediments. Anal Chim Acta. 2007;602:202–10. https://doi.org/10.1016/j.aca.2007.09.022.

33. Raposo JC, Villanueva U, Olivares M, Madariaga JM. Determination of humic substances in sediments by focused ultrasound extraction and ultraviolet visible spectroscopy. Microchem J. 2016;128:26–33. https://doi.org/10.1016/j.microc.2016.04.004.

34. Mecozzi M, Amici M, Pietrantonio E, Romanelli G. An ultrasound assisted extraction of the available humic substance from marine sediments. Ultrason Sonochem. 2002;9:11–8. https://doi.org/10.1016/S1350-4177(01)00098-0.

35. Chang RR, Mylotte R, Hayes MHB, McLnerney R, Tzou YM. A comparison of the compositional differences between humic fractions isolated by the IHSS and exhaustive extraction procedures. Naturwissenschaften. 2014;101:197–209. https://doi.org/10.1007/s00114-013-1140-4.

36. Doskočil L, Burdíková-Szewieczková J, Enev V, Kalina L, Wasserbauer J. Spectral characterization and comparison of humic acids isolated from some European lignites. Fuel. 2018;213:123–32. https://doi.org/10.1016/j.fuel.2017.10.114.

37. Karpukhina E, Mikheev I, Perminova I, Volkov D, Proskurnin M. Rapid quantification of humic components in concentrated humate fertilizer solutions by FTIR spectroscopy. J Soils Sediments. 2019;19:2729–39. https://doi.org/10.1007/s11368-018-2133-x.

38. Fernandes AN, Giovanela M, Esteves VI, de Sierra MMS. Elemental and spectral properties of peat and soil samples and their respective humic substances. J Mol Struct. 2010;971:33–8. https://doi.org/10.1016/j.molstruc.2010.02.069.

39. Drosos M, Jerzykiewicz M, Deligiannakis Y. H-binding groups in lignite versus soil humic acids: NICA-Donnan and spectroscopic parameters. J Colloid Interface Sci. 2009;332:78–84. https://doi.org/10.1016/j.jcis.2008.12.023.

40. Drosos M, Jerzykiewicz M, Louloudi M, Deligiannakis Y. Progress towards synthetic modelling of humic acid: peering into the physicochemical polymerization mechanism. Colloids Surf A Physicochem Eng Asp. 2011;389:254–65. https://doi.org/10.1016/j.colsurfa.2011.08.016.

41. Lu XQ, Hanna JV, Johnson WD. Source indicators of humic substances: an elemental composition, solid state 13C CP/MAS NMR and Py-GC/MS Study. Appl Geochem. 2000;15:1019–33. https://doi.org/10.1016/S0883-2927(99)00103-1.

42. Adani F, Genevini P, Tambone F, Montoneri E. Compost effect on soil humic acid: a NMR study. Chemosphere. 2006;65:1414–8. https://doi.org/10.1016/j.chemosphere.2006.03.070.

43. Zhang J, An T, Chi F, Wei D, Zhou B, Hao X, et al. Evolution over years of structural characteristics of humic acids in Black Soil as a function of various fertilization treatments. J Soils Sediments. 2019;19:1959–69. https://doi.org/10.1007/s11368-018-2212-z.

44. Tan KH. Humic matter in soil and the environment: principles and controversies. 2nd ed. Boca Raton: CRC Press; 2014. https://doi.org/10.1201/b17037.

45. Xu JS, Zhao BZ, Chu WY, Mao JD, Olk DC, Zhang JB, et al. Evidence from nuclear magnetic resonance spectroscopy of the processes of soil organic carbon accumulation under long-term fertilizer management. Eur J Soil Sci. 2017;68:703–15. https://doi.org/10.1111/ejss.12445.

46. Liu P, Zhou W, Cui H, Tan J, Cao S. Structural characteristics of humic substances in buried ancient paddy soils as revealed by 13C NMR spectroscopy. Environ Geochem Health. 2019;41:2459–72. https://doi.org/10.1007/s10653-019-00297-4.

47. Arenillas A, Rubiera F, Pis JJ. Simultaneous thermogravimetric-mass spectrometric study on the pyrolysis behaviour of different rank coals. J Anal Appl Pyrolysis. 1999;50:31–46. https://doi.org/10.1016/S0165-2370(99)00024-8.

48. Kucerík J, Kovár J, Pekar M. Thermoanalytical investigation of lignite humic acids fractions. J Therm Anal Calorim. 2004;76:55–65. https://doi.org/10.1023/B:JTAN.0000027803.24266.48.

49. Boguta P, Sokołowska Z, Skic K. Use of thermal analysis coupled with differential scanning calorimetry, quadrupole mass spectrometry and infrared spectroscopy (TG-DSC-QMS-FTIR) to monitor chemical properties and thermal stability of fulvic and humic acids. PLoS ONE. 2017;12:e0189653. https://doi.org/10.1371/journal.pone.0189653.

50. Dell'Abate MT, Benedetti A, Brookes PC. Hyphenated techniques of thermal analysis for characterisation of soil humic substances. J Sep Sci. 2003;26:433–40. https://doi.org/10.1002/jssc.200390057.

51. Li T, Song F, Zhang J, Liu S, Xing B, Bai Y. Pyrolysis characteristics of soil humic substances using TG-FTIR-MS combined with kinetic models. Sci Total Environ. 2020;698:134237. https://doi.org/10.1016/j.scitotenv.2019.134237.

52. Kara F, Adigüzel D, Atmaca U, Çelik M, Naktiyok J. Characterization and kinetics analysis of the thermal decomposition of the humic substance from hazelnut husk. Turk J Chem. 2020;44:1483–94. https://doi.org/10.3906/kim-2004-62.

53. Jos J, Mathew S. Ammonium nitrate as an eco-friendly oxidizer for composite solid propellants: promises and challenges. Crit Rev Solid State Mater Sci. 2017;42:470–98. https://doi.org/10.1080/10408436.2016.1244642.

54. Oxley JC, Kaushik SM, Gilson NS. Thermal decomposition of ammonium nitrate-based composites. Thermochim Acta. 1989;153:269–86. https://doi.org/10.1016/0040-6031(89)85441-3.

55. Kaniewski M, Hoffmann K, Hoffmann J. Influence of selected potassium salts on thermal stability of ammonium nitrate. Thermochim Acta. 2019;678:178313. https://doi.org/10.1016/j.tca.2019.178313.